NANO LETTERS

pubs.acs.org/NanoLett
Letter

Fatigue Response of MoS_2 with Controlled Introduction of Atomic Vacancies

Yolanda Manzanares-Negro, Aitor Zambudio, Guillermo López-Polín, Soumya Sarkar, Manish Chhowalla, Julio Gómez-Herrero, and Cristina Gómez-Navarro*

Cite This: *Nano Lett.* 2023, 23, 10731−10738

ABSTRACT: Fatigue-induced failure resulting from repetitive stress−strain cycles is a critical concern in the development of robust and durable nanoelectromechanical devices founded on 2D semiconductors. Defects, such as vacancies and grain boundaries, inherent in scalable materials can act as stress concentrators and accelerate fatigue fracture. Here, we investigate MoS_2 with controlled atomic vacancies, to elucidate its mechanical reliability and fatigue response as a function of atomic defect density. High-quality MoS_2 demonstrates an exceptional fatigue response, enduring 10^9 cycles at 80% of its breaking strength (13.5 GPa), surpassing the fatigue resistance of steel and approaching that of graphene. The introduction of atomic defect densities akin to those generated during scalable synthesis processes ($\sim 10^{12}$ cm^{-2}) reduces the fatigue strength to half the breaking strength. Our findings also point toward a sudden defect reconfiguration prior to global failure as the primary fatigue mechanism, offering valuable insights into structure−property relationships.

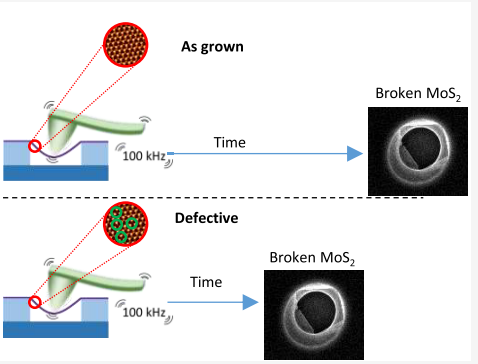

KEYWORDS: *2D materials, TMDCs, fatigue, strain, sulfur vacancies, nanoindentations*

The mechanical endurance of materials is typically limited by their ultimate breaking strength or lifetime due to fatigue induced by cyclic loading at stress below their ultimate tensile strength. Notably, over 80% of fracture incidents occur as a result of fatigue.[1] The achievement of a sustainable future requires the use of durable materials that can withstand repeated mechanical stress. Two-dimensional (2D) materials such as graphene and transition metal dichalcogenides (TMDCs), particularly MoS_2, are being investigated as active components in a variety of electromechanical devices, i.e., flexible displays, mechanical sensors, and nanomechanical resonators,[2,3] due to their unique electronic and mechanical properties, such as appropriate band gap, exceptional electrostatic gate coupling, high flexibility, and ultrahigh strength. While graphene and MoS_2 have been widely employed to enhance the fatigue resistance of bulk materials and structures,[4−7] experimental works into the service life of atomic thin layers have only been conducted in recent years,[8,9] owing to the challenges of performing such experiments. However, with the increasing adoption of few-layered devices in practical applications, their mechanical reliability and service life have become critical concerns.

Similar to bulk materials, the presence of defects, such as atomic vacancies, substitutional atoms, or grain boundaries, modifies the mechanical response of these materials, usually decreasing their intrinsic strength.[10−12] Unfortunately, every scalable method for the production of these materials involves a certain (usually low) density of imperfections in their atomic lattice. Therefore, systematic studies on physical magnitudes upon defect content should enlighten the tolerance of these materials in the road to real life applications.[13]

Here we evaluate the mechanical reliability and fatigue response of MoS_2 by means of indentations with atomic force microscopy (AFM) on suspended membranes. By analyzing multiple breaking events, we determine that monolayered MoS_2 has a reliability similar to engineered ceramics. We demonstrate that the dynamic fatigue life of high-quality CVD grown monolayered MoS_2 is greater than 10^9 cycles for a stress value of 13.5 GPa, which is 0.8 times its ultimate breaking strength. Upon the controlled introduction of atomic vacancies, we perform a systematic study of these magnitudes as a function of defect density. Lateral force microscopy images before and after fatigue testing of the membranes reveal that fatigue results from a sudden defect reconfiguration prior to global failure.

We performed fatigue measurements on MoS_2 monolayer drumheads with diameters ranging from 0.5 to 2 μm. Our starting MoS_2 monolayers were grown by CVD (see SI1) and

Received: July 12, 2023
Revised: November 6, 2023
Accepted: November 8, 2023
Published: November 16, 2023

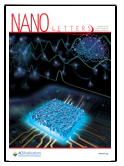

https://doi.org/10.1021/acs.nanolett.3c02479
Nano Lett. 2023, 23, 10731−10738

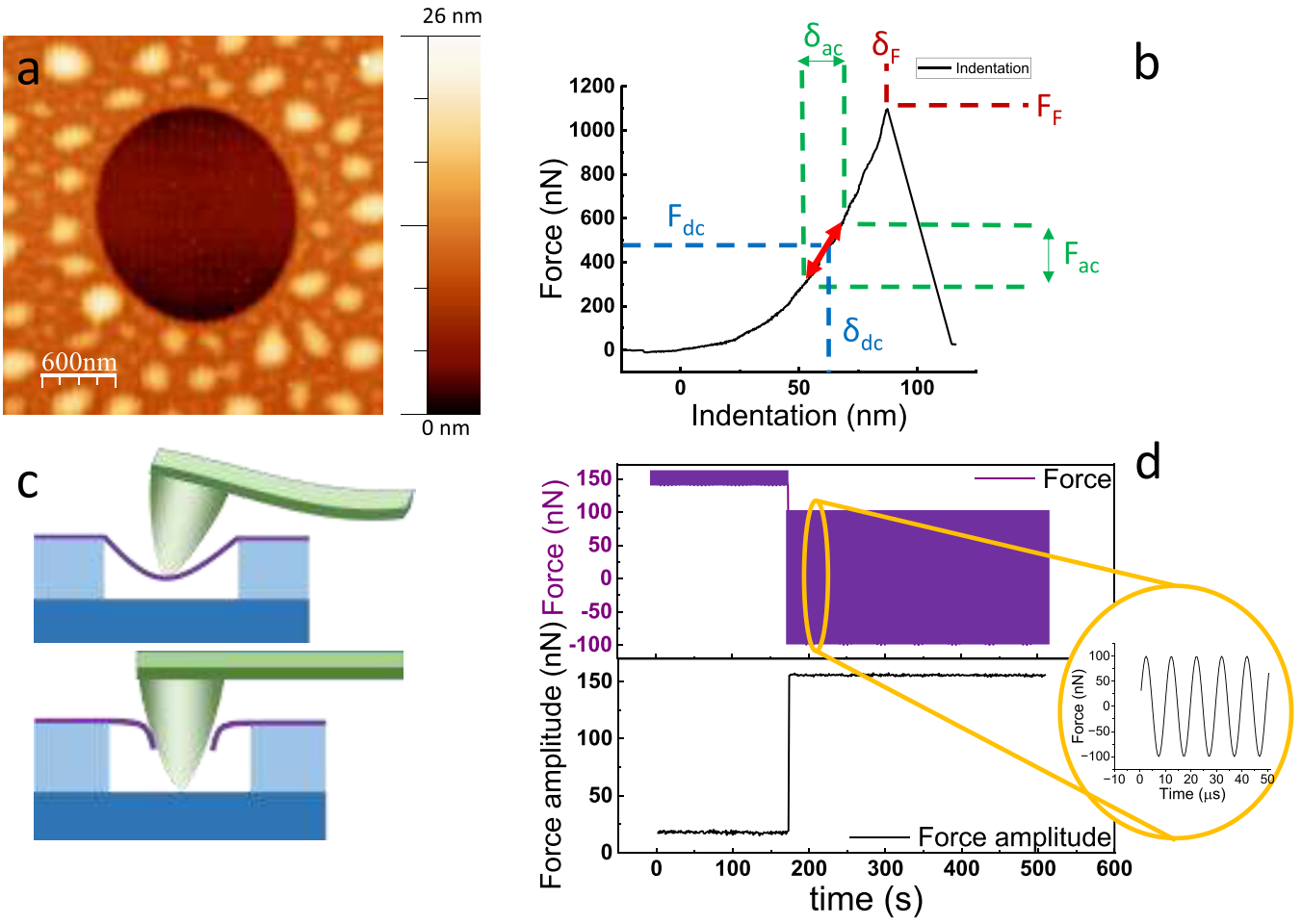

Figure 1. (a) AFM image of a representative MoS_2 microdrum. (b) Force vs indentation curve on a MoS_2 microdrum where the DC and AC forces are marked, along with the corresponding indentation. (c) Upper panel: illustration of an AFM tip indenting a microdrum. Lower panel: sharp decrease in the deflection of the cantilever at the fracture point. (d) Representative data observed near the fracture point. Before failure, the cantilever amplitude is low as a consequence of the reacting force of the suspended membrane. After failure, the cantilever amplitude increases with the free oscillation amplitude.

then transferred by an all-dry technique[14] onto SiO_2/Si substrates with predefined micrometric circular wells yielding suspended membranes of MoS_2 well anchored on the circular perimeter.[15] We confirmed the presence of the MoS_2 monolayers using photoluminescence microscopy[16] (data provided in SI2) and imaged them using AFM in dynamic mode. For this study, we selected only single-layer drumheads exhibiting no observable slack or wrinkling (Figure 1a). We estimated the defect density using micro-Raman spectroscopy (details in SI2).[11,17,18] We obtained native defect densities of 0.4 × 10^{12} and 0.25 × 10^{12} cm^{-2} for two different batches of as-grown samples, corresponding to mean distance between defects of $\langle l_d \rangle$ = 15.7 nm and $\langle l_d \rangle$ = 20 nm, respectively. These defect densities are typical of ultra-high-quality MoS_2 CVD grown samples.[19]

Experiments were performed under ambient conditions (21 °C and ∼30% humidity) using a custom-made AFM. Prior to fatigue testing, we conducted regular indentations at the center of the drumheads. From these indentation curves, we calibrated the force and indentation as shown in Figure 1b and discarded slippering of the MoS_2 at high loading force. We also estimated the elastic modulus of the MoS_2 layers and the residual stress in the membranes yielding values of 200 and ∼0.15 N/m, respectively (see SI3 for details). Subsequently, we applied a static force (with a corresponding static stress σ_{DC}) at the center of the suspended membrane and oscillated the AFM probe at a prefixed amplitude around the static load at a frequency of 100 kHz, inducing a dynamic stress σ_{AC}. We maintained these conditions until fracture. We detected fatigue failure by observing an abrupt increase in the cantilever deflection and a sudden increase in the cantilever amplitude, as shown in Figure 1c,d. We confirmed the membrane failure using AFM images acquired after this event (SI4 fatigue protocol).

Prior to conducting fatigue tests, we indented numerous as-grown MoS_2 monolayer drumheads until they fractured. This allowed us to determine the fracture force of the membranes. Then, we estimated the ultimate breaking strength σ_F using[20]

$$\sigma_F = \sqrt{\frac{E_{2D}F_{break}}{4\pi R_{tip}}} \quad (1)$$

where E_{2D} is the two-dimensional Young's modulus, F_{break} is the fracture force, and R_{tip} is the radius of the indentation tip. This expression ignores nonlinear elasticity, and the derived value is known to overestimate the strength by about 10%; however, it has widely been used in the literature.[21,22] Our measurements yielded an average breaking strength of $\langle \sigma_F \rangle$ = 17 ± 1 GPa, with

https://doi.org/10.1021/acs.nanolett.3c02479
Nano Lett. 2023, 23, 10731−10738

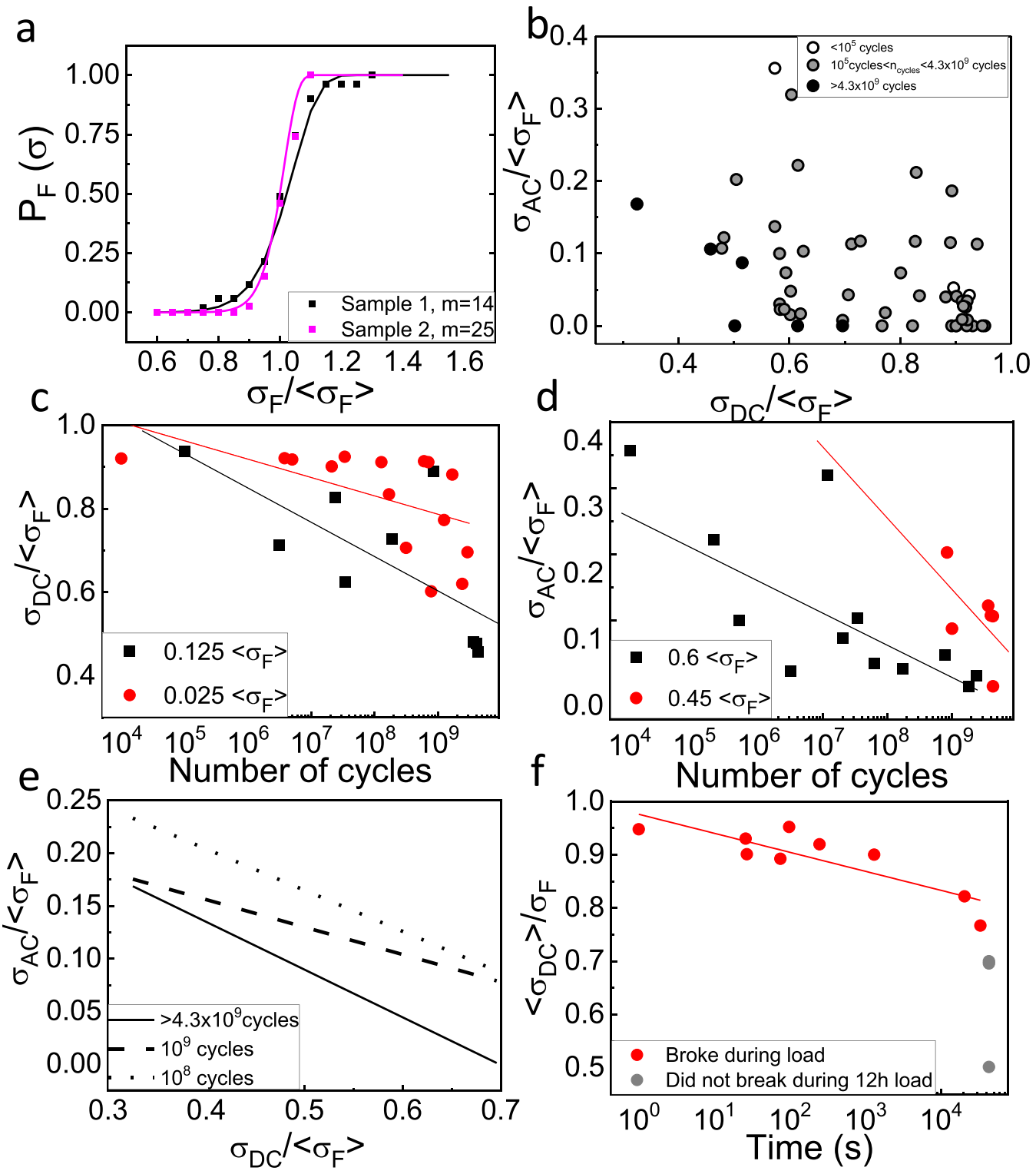

Figure 2. (a) Probability plot of the surveillance of MoS_2 drumheads at different stresses and corresponding Weibull fitting for the two batches of as-grown samples. (b) Goodman diagram representing the applied static (horizontal axis) and dynamic (vertical axis) stress, normalized to the mean breaking strength. Black circles correspond to drumheads that survived after 4.3×10^9 cycles, gray circles represent those that fractured between 1 and 4.3×10^9 cycles, and white dots represent those that broke just after reaching the DC load. (c) S−N diagram with varying σ_{DC} at two different σ_{AC} of $0.125\langle\sigma_F\rangle$ and $0.025\langle\sigma_F\rangle$. (d) S−N diagram of microdrums supporting σ_{AC}/σ_F of $0.6\langle\sigma_F\rangle$ and $0.45\langle\sigma_F\rangle$ with varying σ_{AC}. (e) Goodman lines for microdrums that did not fracture (solid line, lim = $0.45\langle\sigma_F\rangle$, $c = 1.5$), for 10^9 cycles (dashed line, lim = $0.26\langle\sigma_F\rangle$, $c = 1$) and 10^8 cycles (dotted line, lim = $0.36\langle\sigma_F\rangle$, $c = 1.1$). Note that, for nonbroken microdrums, we only provide an upper limit. (f) Static fatigue for as-grown MoS_2. Red dots: microdrums that broke in times lower than 12 h. Gray dots: microdrums that did not break after 12 h of static loading.

no dependence on the residual stress of each membrane (data in SI5), consistent with previous studies.[11,23]

In what follows, all strength values will be normalized to the average ultimate breaking strength of as-grown monolayered

https://doi.org/10.1021/acs.nanolett.3c02479
Nano Lett. 2023, 23, 10731−10738

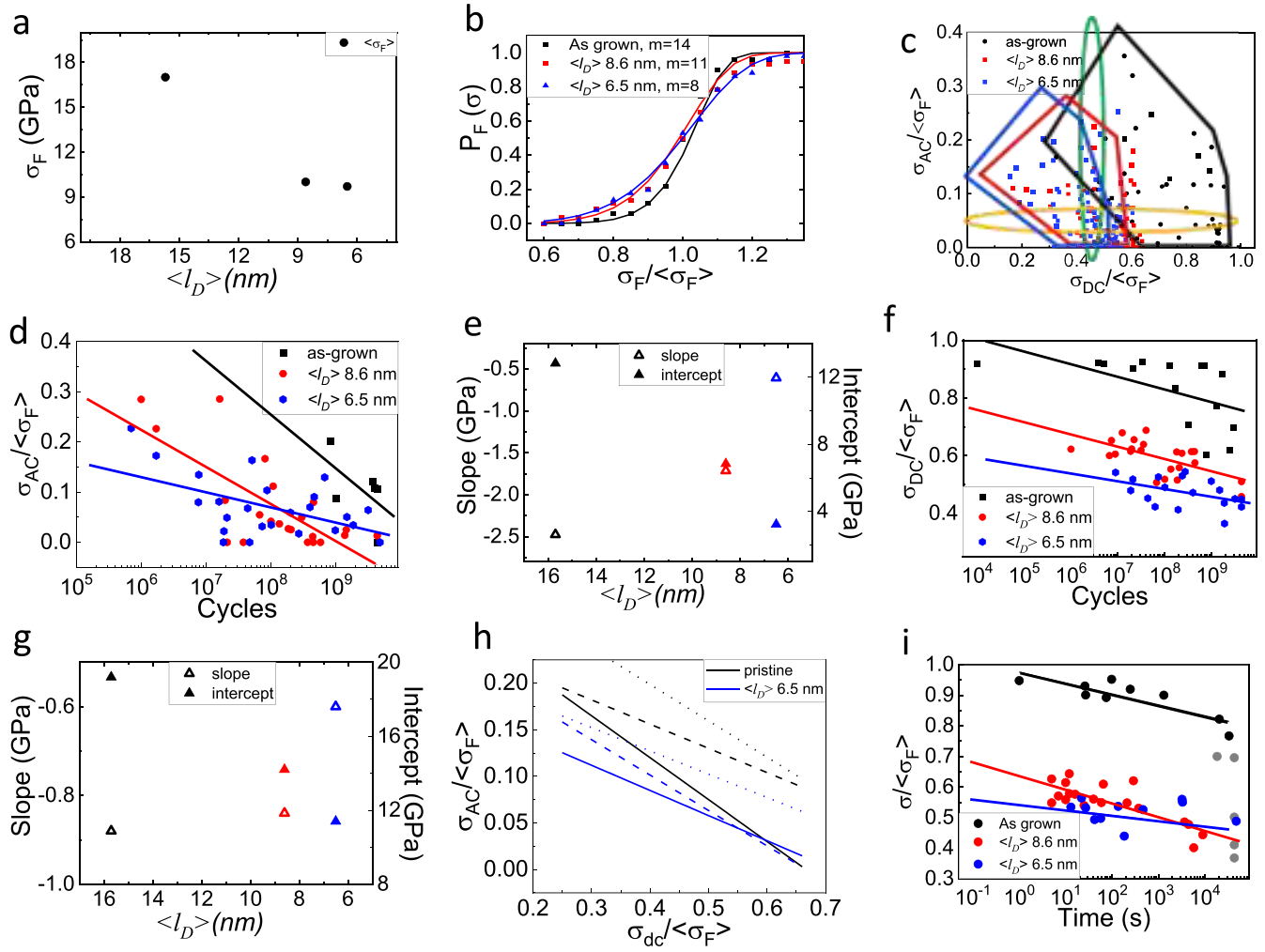

Figure 3. (a) Breaking strength as a function of mean distance between defects. (b) Survival probability and Weibull fitting for as-grown drumheads and those with two consecutive irradiation doses. (c) Goodman diagram showing all results in as-grown and irradiated drumheads. Green and yellow regions indicate the data selected for plots in panels d and f, respectively. (d) Data obtained with a constant σ_{DC} of $0.45\langle\sigma_F\rangle$ and varying σ_{DC}. (e) Intercept and slope of the linear fittings in panel d. (f) Data obtained with a constant σ_{AC} of $0.05\langle\sigma_F\rangle$ and varying σ_{DC}. (g) Intercept and slope of the linear fittings in panel f. (h) Goodman lines for drums that did not break (solid line), those that failed at 10^9 cycles (dashed lines), and microdrums fractured at 10^8 cycles for as-grown (black) and irradiated sample with $\langle l_d\rangle = 6.5$ nm (blue). *(i) Static fatigue lifetime of microdrums with different defect densities. Solid lines are linear fits to the data of the coresponding color.*

MoS_2, i.e., 17 GPa. As shown in Figure 2a, our data are well described by a two-parameter (m, $\langle\sigma_F\rangle$) nanoscale Weibull distribution[24,25]

$$P_F(\sigma_F) = 1 - e^{-(\sigma_F/\langle\sigma_F\rangle)^m} \quad (2)$$

where σ_F is the fracture strength measured for each indentation and $\langle\sigma_F\rangle$ is the average value for all σ_F measured in the experiments.

We characterized two batches of as-grown drumheads with the above-mentioned native defect densities finding Weibull modulus values of $m = 14$ and $m = 25$, for $\langle l_d\rangle = 15.7$ nm and $\langle l_d\rangle = 20$ nm, respectively. The Weibull modulus describes the variability in material strength, and in bulk materials, it is used as an indicator of mechanical reliability. Although the direct applicability of this analysis to nanostructures still has some limitations (detailed discussion in SI6), we compared our results to those reported previously. Our Weibull modulus is lower than the typical values for metals ($m \sim 100$) and that reported for graphene ($m \sim 16$–44).[8,21] However, it is higher than that of the best-engineered ceramics ($m \sim 10$) and similar to that reported for as-grown MoS_2 in a very recent study ($m \sim 22$).[26]

We performed fatigue characterization by applying σ_{DC} and σ_{AC} and measuring the number of cycles for drumhead survival before failure. We used Goodman diagrams to visualize fracture statistics. Figure 2b shows our data of as-grown monolayer MoS_2, where black dots represent the membranes that did not break after 4.3×10^9 loading cycles and white dots represent those that failed right after reaching the load conditions. From this plot, we extracted stress-number of cycles (S−N) graphs performed at a constant σ_{AC} and varying σ_{DC} and at a constant σ_{DC} and varying σ_{AC}. These results are depicted in Figure 2c,d, respectively, where the fatigue life of MoS_2 is shown to be strongly dependent on both σ_{DC} and σ_{AC}.

Our data reveal a fatigue strength of $0.8\langle\sigma_F\rangle$ for 10^9 cycles. These results place high-quality CVD grown MoS_2 as one of the best materials in terms of dynamic fatigue response, with a high level of survival, 1 order of magnitude higher than those of high-strength steels in absolute and relative terms. The best alloys show a fatigue endurance of about $0.5\langle\sigma_F\rangle$, corresponding to 0.5

https://doi.org/10.1021/acs.nanolett.3c02479
Nano Lett. 2023, 23, 10731−10738

GPa for the case of steel. As-grown MoS_2 also exceeds by far the fatigue lifetime of other nanostructures such as Si nanobeams..[27,28] Comparable values to those reported here have been recently reported only for graphene.[8] It is worth noting that our normalized S−N plots superpose those of graphene (see SI7).

We can also define Goodman lines from our data. These lines define the regions where the membranes do not break after a certain number of fatigue cycles and are commonly expressed as[29]

$$\frac{\sigma_{DC}}{\sigma_F} + \frac{\sigma_{AC}}{\sigma_{lim}} = \frac{1}{c} \quad (3)$$

where the parameter σ_{lim} is the maximum σ_{AC} that the material can withstand without breaking, when $\sigma_{DC} = 0$. Additionally, c is known as the safety factor, which indicates how many times a component is safer than what is required for a given use.[30] For the case of 4.3×10^9 cycles, we obtain $\sigma_{lim} = 0.45\langle\sigma_F\rangle$ (7.7 GPa) and $c = 1.5$. Goodman lines for 4.3×10^9, 10^9, and 10^8 cycles, as depicted in Figure 2e, show a very high tolerance to a large number of cycles, a characteristic that is only achieved by metal alloys.

Scanning electron images of the membranes fractured by fatigue tests showed micrometer length tears with straight and sharp edges (starting at the center of the drumhead and reaching the walls of the wells) and crack propagation along crystallographic directions, indicating global and catastrophic failure (Images provided in SI8). For those drumheads that survived 4.3×10^9 cycles, AFM topography images after fatigue testing did not show any evident change. Moreover, subsequent indentations also depicted similar breaking strength and elastic response to the nonirradiated membranes. Since the strength of two-dimensional materials is highly dependent on the size of defects,[11] this result suggests that the dimension of flaws in the most strained region (under the tip) rarely undergo significant alterations during the fatigue process and point toward an abrupt atomistic mechanism of fatigue without progressive damage. It also poses dynamic fatigue proof testing as a noninvasive technique as an approach for high reliability sample selection.

We expanded our dynamic fatigue study to incorporate static loading conditions, which is a key factor in determining the service life of materials. These results are included in Figure 2f.

In classical fracture mechanics, fatigue cracks start at the site of the highest local stress in a device.[1] In macrostructures, this usually happens at the holes or notches. In microstructures, these are inclusions, voids, cavities, or scratches. For highly crystalline atomically thick materials such as TMDCS, imperfections in the atomic lattice are the expected root cause of fatigue initiation. The most common atomic defect in MoS_2 are single sulfur vacancies,[19,31,32] which are inherent in any large-scale production method due to their low defect formation energy.[33] Single sulfur vacancies reduce the strength of MoS_2 and increase fracture toughness.[11] However, the influence of defects on the fatigue lifetime is still unexplored. In what follows, we report our results on this topic.

We produced MoS_2 samples with a controlled type and defect density by irradiating samples with doses of Ar^+ at 500 eV with perpendicular incidence at different irradiation doses. The techniques used to characterize the samples are described in our previous study[11] and SI2. Summarizing, irradiation generated homogeneous densities of vacancies, mainly sulfur monovacancies (~80% of created defects), and a smaller percentage of single Mo vacancies and double sulfur vacancies. Consecutive doses resulted in higher defect densities. We estimated defect densities of 0.4×10^{12} cm^{-2} for the as-grown sample and 1.4 and 2.4×10^{12} cm^{-2} for two consecutive irradiations, corresponding to mean defect distances of $\langle l_d\rangle = 15.7$ nm, $\langle l_d\rangle = 8.6$ nm, and $\langle l_d\rangle = 6.5$ nm, respectively.

Fatigue response of samples with controlled densities of atomic vacancies is depicted in Figure 3. To enable direct comparison, we also included the results for as-grown MoS_2 in these plots. Figure 3a shows that the ultimate breaking strength of the irradiated samples decreased from 17 GPa for the as-grown samples to 10 and 9.7 GPa for the two consecutive irradiation doses, as previously reported.[11] Weibull plots in Figure 3b, show that introduction of atomic vacancies decreases reliability by decreasing Weibull modulus from $m \sim 14$ for the as-grown samples to $m \sim 11$ and $m \sim 8$ for the two irradiated batches of samples, respectively, showing a clear trend. However, it should be noted that the observed decrease in Weibull modulus measured by nanoindentations cannot be directly extrapolated to globally stressed samples (see SI6 for a detailed discussion).

The Goodman diagram in Figure 3c summarizes the results of dynamic fatigue tests conducted on both pristine and irradiated drumheads. The measurements obtained with constant σ_{DC}, enclosed in the green ellipse of Figure 3c, are presented in Figure 3d, with similar plots available in SI9. Linear fits are drawn as continuous lines. Despite the dispersion of experimental data in irradiated samples due to the stochastic nature of brittle failure in MoS_2, the representation of slopes and intercepts with the y-axis of linear fits in Figure 3d reveals a robust trend, as shown in Figure 3e. The y-axis intercept indicates the maximum sustainable value of σ_{AC}, which decreases from 12 to 6 and 3 GPa as the defect density increases. The slope reflects the sensitivity of fracture strength to the number of cycles or the change in survival stress per order of magnitude in the number of cycles. Figure 3f illustrates the lifespan of the samples with a fixed σ_{AC} of $0.125\langle\sigma_F\rangle$ (encircled by the yellow ellipse in Figure 3c). It is evident from the plot that the survival cycles at a constant σ_{AC} decrease with increasing defect density. Again, the slopes and y-axis intercepts are presented in Figure 3g, demonstrating robust trends, as seen in Figure 3e,g. These trends permit the extrapolation of the fatigue response for densities of atomic vacancies within the standard range for MoS_2 produced by scalable methods. Interestingly, we did not observe a fatigue endurance neither for pristine nor for defective drumheads.

Based on our results, the fracture strength at 10^9 cycles appears to be a suitable comparison point for samples with varying densities of atomic vacancies. As-grown MoS_2 displays a fatigue strength of $0.8\langle\sigma_F\rangle$ ($\sigma_{DC} = 13.6$ GPa, $\sigma_{AC} = 0.45$ GPa), which decreases to $0.6\langle\sigma_F\rangle$ ($\sigma_{DC} = 10.2$ GPa, $\sigma_{AC} = 0.45$ GPa) and $0.5\langle\sigma_F\rangle$ ($\sigma_{DC} = 8.5$ GPa, $\sigma_{AC} = 0.45$ GPa) with the introduction of 1.4×10^{12} and 2.4×10^{12} cm^{-2} of atomic defect densities, primarily sulfur vacancies. This line of reasoning allows for the plotting of Goodman lines to define safety regions for both as-grown and irradiated samples. Figure 3h illustrates these lines for the as-grown and most irradiated sample. In the case of the irradiated sample with 2.4×10^{12} cm^{-2} ($\langle l_d\rangle = 6.5$ nm), Goodman lines at 4.3×10^9 cycles yield $\sigma_{lim} = 0.27$ (4.6 GPa) and $c = 1.4$. These safety lines, even for irradiated samples, demonstrate the high fatigue resistance of MoS_2 relative to the best bulk materials, such as high-strength steel. Goodman lines for steel at 10^7 cycles are in the range of hundreds of MPa, implying an improvement of 2 orders of magnitude in the number of cycles and 1 order of magnitude in typical stresses.

https://doi.org/10.1021/acs.nanolett.3c02479
Nano Lett. 2023, 23, 10731−10738

In Figure 3i, we observe a trend of diminishing breaking strength over extended periods of static loading with decreasing breaking stresses for increasing defect density. This observation points out the influence of thermal fluctuations under ambient conditions, which mimic the effects of small-amplitude stress cycles but at a much higher frequency. To draw a comparative perspective, considering a characteristic phonon frequency of 10^{13} Hz for thermal fluctuations, for a given $\sigma_{DC}/\langle\sigma_F\rangle$ achieving membrane failure due to thermal fluctuations would require 10^8 cycles more than those induced by $\sigma_{AC} = 0.05\langle\sigma_F\rangle$, as expected for picometer-sized fluctuation caused by phonons at room temperature. This outcome aligns with prior research, corroborating that thermal fluctuations, while exerting a lesser impact than induced cycling, can indeed contribute to the rupture of covalent bonds when subjected to applied stress levels below the fracture threshold.[8,26]

The failure time τ for a material under an applied stress was described decades ago for polymers by Zurkhov et al.[34] using the qualitative relation $\tau(\sigma) = \tau_0 e^{U_0 - \gamma\sigma/kT}$, where τ_0 is the reciprocal of the natural frequency of the atoms (about 10^{13} Hz), U_0 is the average energy required to break atomic bonds, and γ is a coefficient that translates stress to energy and proportionally decreases with the disorder. By fitting the data to this expression, we obtained an average binding energy of 190 kJ/mol for the as-grown samples, which is comparable to the value of 160 kJ/mol for sulfur bonds in bulk MoS_2, suggesting that this empirical model can also be extrapolated to covalent materials. As expected, we also found that γ and U_0 decrease with an increase in defect density.

Scanning electron microscopy images of irradiated samples after fatigue failure also showed tears propagating to the edge of the wells. A batch of samples was subjected to a fatigue test almost reaching their expected failure conditions, according to graphs depicted in Figure 3d,f. These membranes did not show changes in elastic response neither obvious topographic change after fatigue testing. However, regular AFM topographic images acquired in dynamic mode do not provide enough resolution to resolve atomic scale processes. To gain further insight into the atomistic mechanism of fatigue, we also performed lateral force microscopy (LFM) images of some membranes before and after fatigue testing (see SI10 for conditions). LFM has been shown to resolve single atomic defects when applied to 2D materials;[35] vacancy-type defects in MoS_2 appear in LFM images as high frictional regions. Figure 4 panels a and b depict LFM images of a MoS_2 drumhead with an induced density of defects of 1.4 cm^2 (i.e., $\langle l_d\rangle = 8.6$ nm), where defects appear as darker regions in the image. This membrane was subjected to fatigue testing approaching their expected failure conditions (5×10^6 cycles with $\sigma_{DC} = 0.7\langle\sigma_F\rangle$ and $\sigma_{AC} = 0.2\langle\sigma_F\rangle$), and subsequently imaged again by LFM in the same conditions and using the same AFM probe, within a time interlap of few hours after fatigue testing. For this membrane we did observe at least one detectable change. As highlighted in Figure 4c,d, after fatigue testing, we observed a dark feature that revealed the emergence of a multiatomic defect. Among the seven membranes measured using this protocol, only one of them (that depicted in Figure 4) showed detectable changes. Although LFM can provide atomic resolution and resolve individual vacancies in small images, it is very difficult to account for these defects across the entire suspended membrane. Darker regions in these images are likely double sulfur, or molybdenum vacancies rather than sulfur monovacancies. Despite this issue, our results support previous

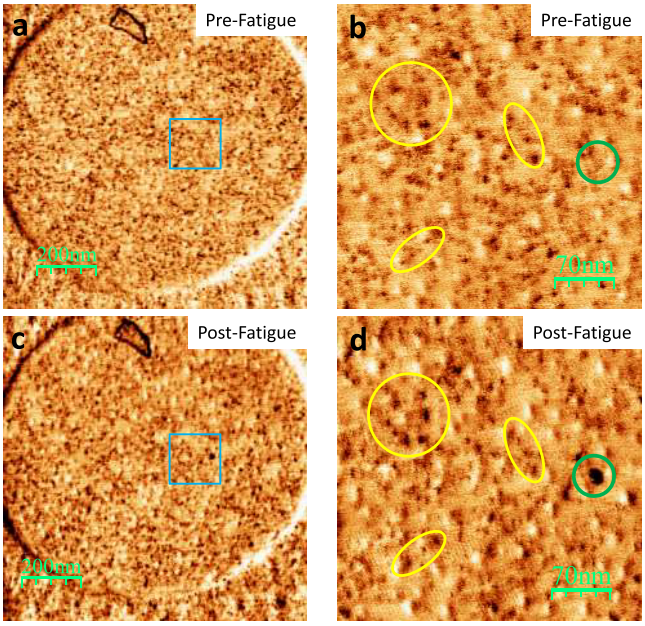

Figure 4. (a) 1024×1024 pixel LFM image of a MoS_2 drumhead with a defect density of 1.4 cm^2 (i.e., $\langle l_d\rangle = 8.6$ nm). (b) LFM of the region marked with a blue square in panel b. Yellow ellipses encircle regions that allowed localizing the desire region before and after fatigue testing and highlight regions where changes were not observed. Green circle guides the eye where the change were observed. (c) 1024×1024 LFM image of the same drumhead shown in panel a but after performing fatigue testing for 4×10^6 cycles with σ_{DC} of $0.7\langle\sigma_F\rangle$ and σ_{AC} of $0.2\langle\sigma_F\rangle$. (d) LFM of the region marked with a blue square in panel c. As every scanning probe microscopy, LFM images are highly dependent on the precise atomic status of the tip apex; this accounts for slight deviations between pre- and postfatigue images (usually changes in contrast and position of the features). However, the emergent darker region comparing between images in panels c and d cannot be ascribed to tip changes.

molecular dynamic simulations[8] where failure upon fatigue in graphene is shown to be preceded by stress mediated bond reconfiguration at vacancy defects and clustering of atomic vacancies into multiatomic ones. The fact that we only observe these changes in a reduced number of membranes also supports the idea of an abrupt atomistic mechanism of fatigue, very different from the progressive damage observed in conventional materials.

Very recent molecular dynamic simulations concluded that the reliability of MoS_2 results from a cooperative effect of three major ingredients: defect configuration, defect density, and thermal fluctuations.[26] Our results quantify the influence of the density of atomic defects and point toward a non-negligible influence of thermal fluctuations upon static loading. The influence of defect configuration cannot be directly derived from the present results, but we envision creation of different kind of atomic defects, such as multivacancy, by Ga irradiation under a field ion beam,[11] or controlled passivation of atomic vacancies[36] to further explore the relevance of defect configuration.

Summarizing, by means of nanomechanical indentations with an AFM tip, we evaluated the mechanical reliability, dynamic and static fatigue lifespan, and safety regions of monolayered MoS_2. A controlled introduction of atomic vacancies allowed a systematic study of these magnitudes as a function of defect content. We observe that the mechanical reliability of MoS_2 decreases with defect induction. Dynamic fatigue testing places

https://doi.org/10.1021/acs.nanolett.3c02479
Nano Lett. 2023, 23, 10731−10738

MoS_2 as one of the best materials showing ultrahigh dynamic fatigue strength, with a strain tolerance at 10^9 cycles and fatigue safety lines achieved only before by graphene and metal alloys. This tolerance decreases with defect introduction, but even the most defective samples evaluated here yet exhibit a fatigue response and safety lines comparable to metal alloys. We also provide insights into the atomistic mechanism of fatigue indicating sudden atomic reconfiguration before global failure. The results presented here, together with previous works reporting improved fracture toughness with controlled defect creation,[11] provide a clear understanding of how atomic defects in monolayer MoS_2 influences its mechanical resilience.

■ ASSOCIATED CONTENT

Supporting Information

The Supporting Information is available free of charge at https://pubs.acs.org/doi/10.1021/acs.nanolett.3c02479.

SI1, CVD growth of MoS_2; SI2, photoluminescence and Raman spectra of MoS_2; SI3, elastic characterization by nanoindentation prior to fatigue testing; SI4, fatigue protocol; SI5, dependence of breaking strength with prestress of the samples; SI6, Weibull distribution; SI7, comparison of fatigue response of MoS_2 and graphene; SI8, scanning electron microcopy images of MoS_2 membranes fractured by fatigue; SI9, complementary S−N plots; SI10m lateral force microscopy details (PDF)

■ AUTHOR INFORMATION

Corresponding Author

Cristina Gómez-Navarro − *Departamento de Física de la Materia Condensada, Universidad Autónoma de Madrid, Cantoblanco 28049, Spain; IFIMAC, Universidad Autónoma de Madrid, Cantoblanco 28049, Spain;* orcid.org/0000-0002-5609-3387; Email: cristina.gomez@uam.es

Authors

Yolanda Manzanares-Negro − *Departamento de Física de la Materia Condensada, Universidad Autónoma de Madrid, Cantoblanco 28049, Spain*

Aitor Zambudio − *Departamento de Física de la Materia Condensada, Universidad Autónoma de Madrid, Cantoblanco 28049, Spain;* orcid.org/0000-0002-3193-7934

Guillermo López-Polín − *Departamento de Física de Materiales, Universidad Autónoma de Madrid, Cantoblanco 28049, Spain;* orcid.org/0000-0001-7187-1733

Soumya Sarkar − *Department of Materials Science and Metallurgy, University of Cambridge, CB30FS Cambridge, U.K.;* orcid.org/0000-0002-9715-9004

Manish Chhowalla − *Department of Materials Science and Metallurgy, University of Cambridge, CB30FS Cambridge, U.K.;* orcid.org/0000-0002-8183-4044

Julio Gómez-Herrero − *Departamento de Física de la Materia Condensada, Universidad Autónoma de Madrid, Cantoblanco 28049, Spain; IFIMAC, Universidad Autónoma de Madrid, Cantoblanco 28049, Spain;* orcid.org/0000-0001-8583-8061

Complete contact information is available at: https://pubs.acs.org/10.1021/acs.nanolett.3c02479

Author Contributions

The manuscript was written through contributions of all authors. All authors have given approval to the final version of the manuscript.

Funding

Ministerio de Ciencia e Investigación through the "María de Maeztu" Programme for Units of Excellence (Grant No. CEX2018-000805-M) and through Grants PID2022-142331NB-I00, PID2022-138908NB-C32, and PID2019-106268GB-C31. Comunidad Autónoma de Madrid through Grants No. S2018/NMT-4321, S2018/NMT-4511.

Notes

The authors declare no competing financial interest.

■ REFERENCES

(1) Zerbst, U.; Madia, M.; Klinger, C.; Bettge, D.; Murakami, Y. Defects as a Root Cause of Fatigue Failure of Metallic Components. I: Basic Aspects. *Engineering Failure Analysis* **2019**, *97*, 777−792.

(2) Li, N.; Wang, Q.; Shen, C.; Wei, Z.; Yu, H.; Zhao, J.; Lu, X.; Wang, G.; He, C.; Xie, L.; Zhu, J.; Du, L.; Yang, R.; Shi, D.; Zhang, G. Large-Scale Flexible and Transparent Electronics Based on Monolayer Molybdenum Disulfide Field-Effect Transistors. *Nat. Electron* **2020**, *3* (11), 711−717.

(3) Ganatra, R.; Zhang, Q. Few-Layer MoS2: A Promising Layered Semiconductor. *ACS Nano* **2014**, *8* (5), 4074−4099.

(4) Rafiee, M. A.; Rafiee, J.; Srivastava, I.; Wang, Z.; Song, H.; Yu, Z.-Z.; Koratkar, N. Fracture and Fatigue in Graphene Nanocomposites. *Small* **2010**, *6* (2), 179−183.

(5) Parente, J. M.; Santos, P.; Valvez, S.; Silva, M. P.; Reis, P. N. B. Fatigue Behaviour of Graphene Composites: An Overview. *Procedia Structural Integrity* **2020**, *25*, 282−293.

(6) Guan, H.; Dai, X.; Ni, L.; Hu, J.; Wang, X. Highly Elastic and Fatigue-Resistant Graphene-Wrapped Lamellar Wood Sponges for High-Performance Piezoresistive Sensors. *ACS Sustainable Chem. Eng.* **2021**, *9* (45), 15267−15277.

(7) Baran, Ö. Adhesion and Fatigue Resistance of Ta-Doped MoS2 Composite Coatings Deposited with Pulsed-DC Magnetron Sputtering. *J. Adhes. Sci. Technol.* **2017**, *31* (11), 1181−1195.

(8) Cui, T.; Mukherjee, S.; Sudeep, P. M.; Colas, G.; Najafi, F.; Tam, J.; Ajayan, P. M.; Singh, C. V.; Sun, Y.; Filleter, T. Fatigue of Graphene. *Nat. Mater.* **2020**, *19* (4), 405−411.

(9) Najafi, F.; Wang, G.; Cui, T.; Anand, A.; Mukherjee, S.; Filleter, T.; Sain, M.; Singh, C. V. Fatigue Resistance of Atomically Thin Graphene Oxide. *Carbon* **2021**, *183*, 780−788.

(10) López-Polín, G.; Gómez-Navarro, C.; Parente, V.; Guinea, F.; Katsnelson, M. I.; Pérez-Murano, F.; Gómez-Herrero, J. Increasing the Elastic Modulus of Graphene by Controlled Defect Creation. *Nature Phys.* **2015**, *11* (1), 26−31.

(11) Manzanares-Negro, Y.; López-Polín, G.; Fujisawa, K.; Zhang, T.; Zhang, F.; Kahn, E.; Perea-López, N.; Terrones, M.; Gómez-Herrero, J.; Gómez-Navarro, C. Confined Crack Propagation in MoS2Monolayers by Creating Atomic Vacancies. *ACS Nano* **2021**, *15* (1), 1210−1216.

(12) Xu, J.; Yuan, G.; Zhu, Q.; Wang, J.; Tang, S.; Gao, L. Enhancing the Strength of Graphene by a Denser Grain Boundary. *ACS Nano* **2018**, *12*, 4529.

(13) Huang, P.; Lukin, R.; Faleev, M.; Kazeev, N.; Al-Maeeni, A. R.; Andreeva, D. V.; Ustyuzhanin, A.; Tormasov, A.; Castro Neto, A. H.; Novoselov, K. S. Unveiling the Complex Structure-Property Correlation of Defects in 2D Materials Based on High Throughput Datasets. *npj 2D Mater. Appl.* **2023**, *7* (1), 1−10.

(14) Castellanos-Gomez, A.; Buscema, M.; Molenaar, R.; Singh, V.; Janssen, L.; van der Zant, H. S J; Steele, G. A Deterministic Transfer of Two-Dimensional Materials by All-Dry Viscoelastic Stamping. *2D Mater.* **2014**, *1* (1), 011002.

(15) Koenig, S. P.; Boddeti, N. G.; Dunn, M. L.; Bunch, J. S. Ultrastrong Adhesion of Graphene Membranes. *Nat. Nanotechnol.* **2011**, *6* (9), 543−546.

https://doi.org/10.1021/acs.nanolett.3c02479
Nano Lett. 2023, 23, 10731−10738

(16) Splendiani, A.; Sun, L.; Zhang, Y.; Li, T.; Kim, J.; Chim, C.-Y.; Galli, G.; Wang, F. Emerging Photoluminescence in Monolayer MoS2. *Nano Lett.* **2010**, *10* (4), 1271−1275.
(17) Mignuzzi, S.; Pollard, A. J.; Bonini, N.; Brennan, B.; Gilmore, I. S.; Pimenta, M. A.; Richards, D.; Roy, D. Effect of Disorder on Raman Scattering of Single-Layer Mo S 2. *Phys. Rev. B* **2015**, *91* (19), 195411.
(18) Fujisawa, K.; Carvalho, B. R.; Zhang, T.; Perea-López, N.; Lin, Z.; Carozo, V.; Ramos, S. L. L. M.; Kahn, E.; Bolotsky, A.; Liu, H.; Elías, A. L.; Terrones, M. Quantification and Healing of Defects in Atomically Thin Molybdenum Disulfide: Beyond the Controlled Creation of Atomic Defects. *ACS Nano* **2021**, *15* (6), 9658−9669.
(19) Hong, J.; Hu, Z.; Probert, M.; Li, K.; Lv, D.; Yang, X.; Gu, L.; Mao, N.; Feng, Q.; Xie, L.; Zhang, J.; Wu, D.; Zhang, Z.; Jin, C.; Ji, W.; Zhang, X.; Yuan, J.; Zhang, Z. Exploring Atomic Defects in Molybdenum Disulphide Monolayers. *Nat. Commun.* **2015**, *6* (1), 6293.
(20) Begley, M. R.; Mackin, T. J. Spherical Indentation of Freestanding Circular Thin Films in the Membrane Regime. *Journal of the Mechanics and Physics of Solids* **2004**, *52* (9), 2005−2023.
(21) Lee, C.; Wei, X.; Kysar, J. W.; Hone, J. Measurement of the Elastic Properties and Intrinsic Strength of Monolayer Graphene. *Science* **2008**, *321* (5887), 385−388.
(22) Bertolazzi, S.; Brivio, J.; Kis, A. Stretching and Breaking of Ultrathin MoS2. *ACS Nano* **2011**, *5* (12), 9703−9709.
(23) Castellanos-Gomez, A.; Poot, M.; Steele, G. A.; van der Zant, H. S.; Agraït, N.; Rubio-Bollinger, G. Mechanical Properties of Freely Suspended Semiconducting Graphene-like Layers Based on MoS2. *Nanoscale Res. Lett.* **2012**, *7* (1), 233.
(24) Weibull, W. A Statistical Distribution Function of Wide Applicability. *Journal of Applied Mechanics* **1951**, *18* (3), 293−297.
(25) Pugno, N. M.; Ruoff, R. S. Nanoscale Weibull Statistics. *J. Appl. Phys.* **2006**, *99* (2), 024301.
(26) Cui, T.; Mukherjee, S.; Onodera, M.; Wang, G.; Kumral, B.; Islam, A.; Shayegannia, M.; Krishnan, G.; Barri, N.; Serles, P.; Zhang, X.; Sassi, L. M.; Tam, J.; Bassim, N.; Kherani, N. P.; Ajayan, P. M.; Machida, T.; Singh, C. V.; Sun, Y.; Filleter, T. Mechanical Reliability of Monolayer MoS2 and WSe2. *Matter* **2022**, *5* (9), 2975−2989.
(27) Namazu, T.; Isono, Y. Fatigue Life Prediction Criterion for Micro-Nanoscale Single-Crystal Silicon Structures. *Journal of Microelectromechanical Systems* **2009**, *18* (1), 129−137.
(28) Sundararajan, S.; Bhushan, B. Development of AFM-Based Techniques to Measure Mechanical Properties of Nanoscale Structures. *Sensors and Actuators A: Physical* **2002**, *101* (3), 338−351.
(29) Goodman, J. *Mechanics Applied to Engineering*; London [etc.] Longmans, Green & Co., 1914.
(30) *Standard Handbook of Machine Design*, 2nd ed.; Shigley, J. E., Mischke, C. R., Eds.; McGraw-Hill: New York, 1996.
(31) KC, S.; Longo, R. C.; Addou, R.; Wallace, R. M.; Cho, K. Impact of Intrinsic Atomic Defects on the Electronic Structure of MoS2Monolayers. *Nanotechnology* **2014**, *25* (37), 375703.
(32) Roy, A.; Ghosh, R.; Rai, A.; Sanne, A.; Kim, K.; Movva, H. C. P.; Dey, R.; Pramanik, T.; Chowdhury, S.; Tutuc, E.; Banerjee, S. K. Intra-Domain Periodic Defects in Monolayer MoS2. *Appl. Phys. Lett.* **2017**, *110* (20), 201905.
(33) Ghorbani-Asl, M.; Kretschmer, S.; Spearot, D. E.; Krasheninnikov, A. V. Two-Dimensional MoS_2 under Ion Irradiation: From Controlled Defect Production to Electronic Structure Engineering. *2D Mater.* **2017**, *4* (2), 025078.
(34) Zhurkov, S. N. Kinetic Concept of the Strength of Solids. *Int. J. Fract.* **1984**, *26* (4), 295−307.
(35) Zambudio, A.; Gnecco, E.; Colchero, J.; Pérez, R.; Gómez-Herrero, J.; Gómez-Navarro, C. Fine Defect Engineering of Graphene Friction. *Carbon* **2021**, *182*, 735−741.
(36) Sivaram, S. V.; Hanbicki, A. T.; Rosenberger, M. R.; Jernigan, G. G.; Chuang, H.-J.; McCreary, K. M.; Jonker, B. T. Spatially Selective Enhancement of Photoluminescence in MoS2 by Exciton-Mediated Adsorption and Defect Passivation. *ACS Appl. Mater. Interfaces* **2019**, *11* (17), 16147−16155.

https://doi.org/10.1021/acs.nanolett.3c02479
Nano Lett. 2023, 23, 10731−10738